OPEN ACCESS
IOP Publishing
Journal of Physics D: Applied Physics
J. Phys. D: Appl. Phys. **57** (2024) 405207 (16pp)
https://doi.org/10.1088/1361-6463/ad5f3b

A hierarchal model for bacterial cell inactivation in solution by direct and indirect treatment using cold atmospheric plasmas

Jordyn Polito[1] **and Mark J Kushner**[2,*]

[1] Department of Chemical Engineering, University of Michigan, Ann Arbor, MI 48109, United States of America
[2] Department of Electrical Engineering and Computer Science, University of Michigan, Ann Arbor, MI 48109, United States of America

E-mail: mjkush@umich.edu and jopolito@umich.edu

Received 14 March 2024, revised 22 May 2024
Accepted for publication 4 July 2024
Published 19 July 2024

Abstract

Cold atmospheric plasma devices have shown promise for a variety of plasma medical applications, including wound healing and bacterial inactivation often performed in liquids. In the latter application, plasma-produced reactive oxygen and nitrogen species (RONS) interact with and damage bacterial cells, though the exact mechanism by which cell damage occurs is unclear. Computational models can help elucidate relationships between plasma-produced RONS and cell killing by enabling direct comparison between dissimilar plasma devices and by examining the effects of changing operating parameters in these devices. In biological applications, computational models of plasma-liquid interactions would be most effective in design and optimization of plasma devices if there is a corresponding prediction of the biological outcome. In this work, we propose a hierarchal model for planktonic bacterial cell inactivation by plasma produced RONS in liquid. A previously developed reaction mechanism for plasma induced modification of cysteine was extended to provide a basis for cell killing by plasma-produced RONS. Results from the model are compared to literature values to provide proof of concept. Differences in time to bacterial inactivation as a function of plasma operating parameters including gas composition and plasma source configuration are discussed. Results indicate that optimizing gas-phase reactive nitrogen species production may be key in the design of plasma devices for disinfection.

Keywords: model, atmospheric pressure plasma, bacterial cell death, plasma-liquid interactions

* Author to whom any correspondence should be addressed.

1. Introduction

Cold atmospheric plasmas (CAP) can provide a non-invasive source of reactive oxygen and nitrogen species (RONS) for a variety of plasma medical and agricultural applications. Current uses of CAP include cancer therapy [1, 2], wound healing [3, 4], surface sterilization [5, 6], air purification [7, 8], and food sanitation [9, 10]. CAP is promising for plasma medical applications, in particular medical instrument sterilization and wound disinfection, as the plasma efficiently kills bacteria while minimizing damage to the treated surface or detrimentally affecting the patient. The mechanisms through which plasma-produced RONS interact with bacteria to promote inactivation are unclear. Refining these mechanisms is made complex by the large variety of commercial and experimental plasma device configurations. This large variety makes it difficult to establish relationships between plasma operating parameters (e.g. gas composition, power, and distance between the plasma source and the target) and biological outcomes. Computational models can help elucidate the relationships between plasma-produced RONS and cell killing by enabling direct comparison between dissimilar plasma devices and operating parameters. In this paper, we report on a hierarchical plasma -induced cell-death model with the goal of establishing these relationships. The intent of this investigation is not to compare to a specific experimental result, but rather to demonstrate a methodology for quantitatively establishing relationships between plasma parameters and biological outcomes.

Several CAP sources have been investigated for plasma medical applications, including atmospheric pressure plasma jet (APPJ) sources [11, 12]. APPJs can be classified as indirect (non-touching) sources in which the plasma is not in contact with the target or as direct (touching) sources in which the plasma is in contact with the target (figure 1). An example of an indirect APPJ is the COST-Jet [13] where the applied electric field is perpendicular to the gas flow, producing a confined plasma and largely neutral plume carrying activated species to the surface. An example of a direct APPJ is the kINPen [4] where the electrode configuration enables propagation of an ionization wave through the gas plume. The proximity of the exit of the APPJ to the surface then determines whether the APPJ is touching or not touching. Typically, these APPJ sources are operated in a carrier gas such as argon or helium containing few percent mixtures of air, water, or oxygen to generate RONS in the gas-phase. Further reactions and RONS production can occur as the rare-gas jet mixes with the ambient air.

Often, the biological target, such as planktonic bacteria, is covered by a layer of liquid or is contained in solution. Both types of sources are efficient at generating RONS in the gas-phase which can solvate into the liquid-phase to produce important antibacterial RONS such as OH_{aq}, H_2O_{2aq}, NO_{3aq}^-, and $ONOO_{aq}^-$. (The aq subscript indicates in liquid, aqueous species.) These species are produced either by the direct solvation of plasma produced species or by subsequent reactions in the liquid.

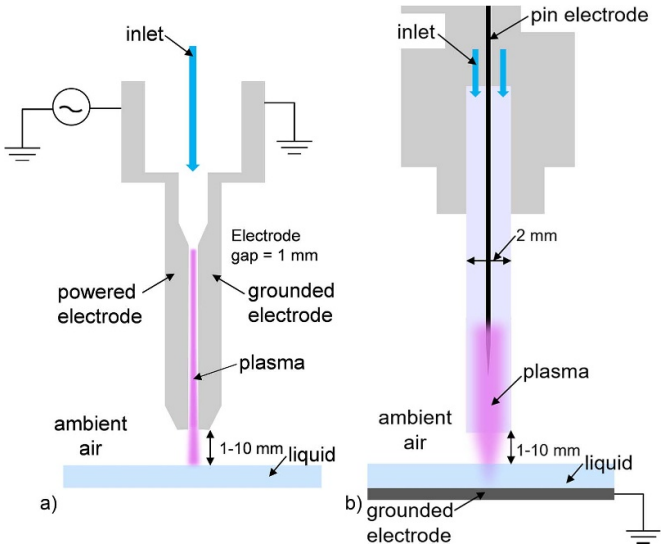

Figure 1. Example of (a) an indirect (non-touching) plasma source and (b) a direct (touching) plasma source.

Many plasma configurations have been studied independently as sources for bacterial inactivation, however there are few direct comparisons between devices. In some studies, direct and indirect treatment are compared using the same device. For example, Yahaya *et al* studied the direct and indirect bactericidal effects of a dielectric barrier discharge by comparing the kill curves of cells exposed directly to the plasma versus those exposed to plasma activated water [14]. They found that while both direct and indirect treatment resulted in reduction of cell viability, direct treatment was more effective and was about fifteen times faster. Others have studied indirect plasma treatment by allowing the plasma effluent (plasma-produced RONS) to come into contact with solution containing bacterial cells. Van Gils *et al* investigated inactivation of the drug-resistant bacteria *Pseudomonas aeruginosa* in solution by argon APPJ. They found that a 6-log reduction in cell viability was achievable after about 3 min of treatment [15].

Researchers have reported the time for bacterial inactivation using direct plasma configurations to be on the order of 3–5 min [16], whereas bacterial inactivation using indirect plasma configurations occurs on the order of 10 min or longer [17]. Shorter time for bacterial inactivation using direct sources is likely partly due to the additional delivery of photons and ions to the liquid surface, which leads to higher generation of RONS by liquid-phase reactions than when indirect sources are used. The time to inactivation will also depend on plasma operating parameters such as power, gas composition, and distance from the target, as well as the initial bacteria concentration.

The precise mechanisms of bacterial inactivation by plasma-produced RONS are still unclear. In general, plasma-induced bacterial inactivation is thought to be due to apoptosis through oxidative stress [12, 18, 19]. Reactions of plasma-produced RONS with organic molecules on the cell membrane

result in interruptions to cell signaling pathways. Damage to the membrane itself or to cell signaling pathways results in excessive uptake of reactive oxygen species (ROS) into the cell body. High concentrations of ROS such as O and OH in the cell body result in reduced functionality of vital cell processes, and eventually lead to cell death.

Determining the mechanism for bacterial inactivation is further complicated in many applications by the bacteria being in a liquid or cell culture medium. For example, plasma devices have been used to reduce bacterial load in severe burn wounds, which are often coated with thin layers of fluid [20, 21]. The presence of a liquid layer, whether produced by the host organism, or in experiments where cells are cultured in solution containing nutrients, affects both the generation and consumption of plasma-produced RONS. The effects of the components of the solution must be considered when determining, for example, the dose of bactericidal RONS necessary to achieve the desired outcome.

Computer models can help elucidate the mechanism of bacterial inactivation by plasma-produced RONS by enabling comparison between plasma source configurations, gas compositions, power profiles, or other operating conditions that may be difficult to experimentally compare side-by-side. To date, models have characterized plasma-production of RONS and delivery of those RONS to the target [22, 23] and have predicted post-treatment modifications of key amino acids [24, 25], but little work has been done to represent the mechanism by which RONS interact with large organic molecules or cells in wet conditions. Previous work has shown success in approximating reaction rates of organic molecules in solution by starting from analogous gas-phase reaction rates of RONS with long-chain alkanes [26]. Since cells membranes are, at the most basic level, surfaces made of organic molecules, it follows that a first approximation to determine a reaction mechanism for RONS with cells may be to start with previous mechanisms for RONS with organic molecules.

In this work, we discuss results from a plasma chemistry and plasma liquid interaction model, and a hierarchical cell death model to describe trends in planktonic cell death resulting from CAP treatment. A mechanism based on CAP treatment of cysteine was adjusted for consistency with cell kill curves in the literature, and is proposed to represent reaction rates for RONS interactions with planktonic bacteria cells in the hierarchical cell death model. Results for time to bacterial inactivation as a function of plasma operating parameters such as gas composition and plasma source configuration are discussed and compared to results from the literature to provide proof of concept. Model results are consistent with the literature and indicate that bacterial inactivation efficiency is higher in systems that generate more reactive nitrogen species (RNS) in the gas phase, and which use touching sources. Descriptions of the global plasma chemistry model and the cell death model are in Section 2. The base case plasma properties are discussed in Section 3. Parametric studies of plasma treatment of planktonic bacteria are discussed in Section 4 and concluding remarks are in Section 5.

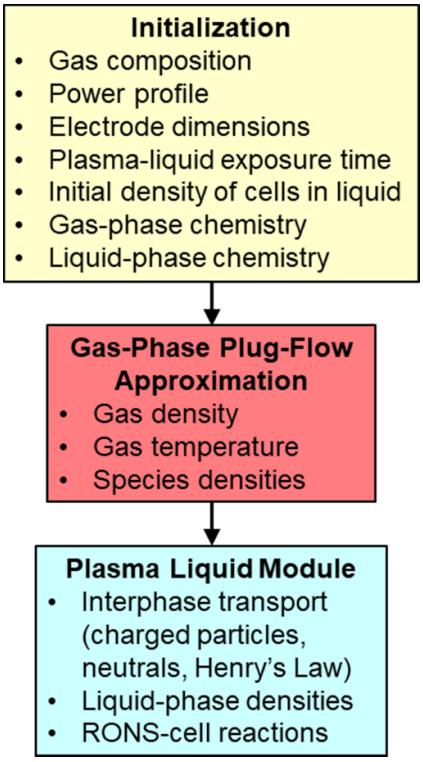

Figure 2. Schematic of *GlobalKin*.

2. Model description

2.1. 0D plasma chemistry model

GlobalKin, the 0D plasma chemistry model used in this investigation, is a dual-phase model with capability for addressing plasma-liquid interactions [23, 27]. Species densities are computed as a function of position in a reactor using a plug-flow approximation in species continuity equations that account for sources and losses due to electron impact, ion-molecule and neutral reactions, diffusion to the walls, and gas flow. The electron temperature is a reactor average or position dependent value (for plug flow) that is given by solving the electron energy equation. The stationary Boltzmann's equation is solved over a range of E/N (electric field/gas number density) values to generate a lookup table of rate and transport coefficients which is interpolated as a function of electron temperature during execution of the code. The lookup table is updated periodically as gas composition changes. A schematic of *GlobalKin* is shown in figure 2.

Gas flow is resolved using a plug-flow approach in which a slug of gas having a cross-sectional area A, equivalent to the reactor cross sectional area, moves down the length of the reactor with a speed that is dependent upon input flow rate, gas density, and A. The speed of the plug is adjusted as total gas number density changes due to gas heating, gas phase reactions, or reactions on walls to maintain constant pressure. Transport to the walls (perpendicular to the flow-direction) is governed by ambipolar diffusion for charged particles and fundamental mode free diffusion for neutral particles. Input power (Wcm^3) is specified in the flow direction as a function

of position along the length of the reactor. When using radio frequency (RF) power, the power is assumed not to be time-varying along the axis. Rather the power is the average over the RF period. Gas flow beyond the boundary of the reactor is described below.

For strictly remote plasma sources, the power density is constant along the length of the reactor except for a 1 mm ramp-up distance at the entrance to the reactor and a 2 mm ramp-down distance at the exit of the reactor. The power density profile is normalized so that the integral over the length of the reactor is equal to the total input power. The power is only deposited in the input gases (and their reaction products) prior to any mixing with the ambient gas. These plasma sources would be non-touching akin to the COST-Jet (figure 1(a)). For extended plasma sources akin to the kINPen (figure 1(b)), the plasma power deposition may penetrate beyond the end of the device into the gap, which is the region between the end of the device and the surface being treated. Extended plasma sources bridging the gap are then touching sources. Power deposition in the gap then results in plasma interactions with ambient gases.

In APPJ configurations used for treating surfaces, the plasma activated plume, here dominated by rare gas, comes into contact with ambient air in the gap before reaching the target. Reactive species then interact with the ambient and, in the case of extended sources, produce additional RONS by electron impact processes with the ambient. In plug-flow mode, ambient air is introduced to the rare gas plume extending beyond the plasma sources to approximate the diffusion of ambient gases into the plume. Computationally this is accomplished with a set of gas inlets injecting humid air ($N_2/O_2/H_2O = 78/20/2$) along the length of the plume in the gap. The injected air flow rate was chosen based on on-going modeling efforts to match the gas-phase production of OH, HO_2, and H_2O_2 in the air gap of the COST-jet, which is in part a function of humidity in the air gap. The flowrate of the air inlets used in this work was between 0.5% and 2% of that of the gas flowing through the plasma source.

The *GlobalKin* liquid module has been described in detail in previous work and so will be discussed only briefly here [23, 27]. *GobalKin* provides fluxes of species to the liquid surface that diffuse to the surface of the liquid across a boundary layer. If the liquid phase analogue of an incident gas phase is not saturated, the gas species will solvate into the liquid with a probability $S_{i,l} = \frac{h_i n_{i,g} - n_{i,l}}{h_i n_{i,g}}$ where h_i is the Henry's law constant for species i, $n_{i,g}$ is the gas-phase density of species i, and $n_{i,l}$ is the liquid-phase density of species i. If the liquid analogue is supersaturated, the liquid phase species desolvates with rate proportional to $S_{i,l} = \frac{n_{i,l} - h_i n_{i,g}}{h_i n_{i,g}}$. Henry's law constants used in this work are the same as reported in [26]. Heavy charged particles and electrons solvate into the liquid with unity probability. Liquid species densities are given by integration of a continuity equation that accounts for sources and losses due to solvation, evaporation, and liquid-phase reactions. A set of reactions was added to the liquid-phase chemistry to describe liquid-phase species interactions with cells, as discussed in the following section.

2.2. Hierarchal model for cell death

The experimental observation is that planktonic bacterial cell death does not begin immediately upon application of the plasma to the solution or growth media. Rather, there is an induction time during which assays show that although cells may be stressed, they are in large part alive [28, 29]. Only after a critical treatment time do cells begin to die. Since reactions of cells with liquid-phase RONS would presumably begin as soon as the solution is activated by the plasma, these observations imply that cell death results from the accumulation of damage, where here damage is defined in the most general way as cells not being healthy. As the cells accumulate damage as a result of reactions with RONS, the cells become stressed. After accumulating a critical amount of damage, the cells die. When removing the source of damage and stress (e.g. turning off the plasma), some fraction of the less stressed or damaged cells may recover to be healthy. Some fraction of the more stressed or damaged cells will die.

A hierarchal reaction mechanism was developed to describe cell death in solution as a result of plasma-produced-RONS delivery to a liquid surface. The hierarchal model is based on a single cell accumulating a critical amount of damage by a sequence of reactions with RONS. In this process, a healthy cell becomes progressively more stressed or sick. When a critical amount of damage has been accumulated, the cell is declared to be dead. Table 1 contains the reaction mechanism that describes this process. A cell that has undergone n sequential reactions with liquid RONS is called the n^{th} generation of the cell. Each generation of the cell, as described below, is treated as a separate species in the model. The sequence of reactions describing the hierarchal cell death process is incorporated into the reaction mechanism. The liquid species continuity equations for each generation of cell are integrated just as any other liquid resident species. The exception is that the cells do not have gas phase analogues, and so interphase transport into and out of the liquid is not included for cells while being included for other liquid phase species.

A typical bacterium is a about a micron in diameter and 2–5 μm long [30, 31]. With a surface site density of 10^{15} cm^{-2}, there are about 10^8 sites on the cell membrane that contain functionalities (e.g. –H, –NH_2, –OH, –O) that are susceptible to attack by RONS. The sequential set of reactions that transition a healthy cell to a sick (or stressed) cell to a dead cell is based on reactions of RONS with these surface functionalities. Modifications of organic molecules, such as proteins, on the cell membrane, may result in changes to cell signaling, motility, or regulatory function that can lead to expedited cell death [12]. Reaction rates for this mechanism were estimated based on rates of hydrogen abstraction from the small organic molecule cysteine by RONS.

Cysteine contains biologically relevant functionalities (–SH, –NH_2, –COOH, –H) and is often used in biological models to quantify complex reaction pathways [32]. Previous work established a reaction mechanism for plasma-assisted modifications of cysteine in solution that was in good agreement with experimental data [26]. Only rates for hydrogen

Table 1. CFU plasma deactivation reaction mechanism.

	Reaction	Reaction rate coefficient ($cm^3 s^{-1}$)
	Cell death reactions[a]	
1	$CFU_i + O_{aq} \rightarrow CFU_{i+1}$	1.68×10^{-15}
2	$CFU_i + O^-_{aq} \rightarrow CFU_{i+1} + e_{aq}$	1.68×10^{-20}
3	$CFU_i + OH_{aq} \rightarrow CFU_{i+1}$	1.68×10^{-17}
4	$CFU_i + OH^-_{aq} \rightarrow CFU_{i+1} + e_{aq}$	1.91×10^{-20}
5	$CFU_i + H_2O_{2aq} \rightarrow CFU_{i+1} + H_2O_{aq}$	4.98×10^{-18}
6	$CFU_i + HO_{2aq} \rightarrow CFU_{i+1}$	5.65×10^{-16}
7	$CFU_i + NO_{aq} \rightarrow CFU_{i+1}$	8.00×10^{-15}
8	$CFU_i + NO^-_{2aq} \rightarrow CFU_{i+1} + e_{aq}$	5.60×10^{-22}
9	$CFU_i + NO^-_{3aq} \rightarrow CFU_{i+1} + e_{aq}$	5.60×10^{-22}
10	$CFU_i + ONOO^-_{aq} \rightarrow CFU_{i+1} + e_{aq}$	5.60×10^{-22}
	Ghost reactions[b,c,d,e,f,g]	
11	$CFU_j + O_{aq} \rightarrow CFU_j$	2.52×10^{-9}
12	$CFU_j + O^-_{aq} \rightarrow CFU_j + e_{aq}$	2.52×10^{-14}
13	$CFU_j + OH_{aq} \rightarrow CFU_j$	2.52×10^{-11}
14	$CFU_j + OH^-_{aq} \rightarrow CFU_j + e_{aq}$	2.87×10^{-14}
15	$CFU_j + H_2O_{2aq} \rightarrow CFU_j + H_2O_{aq}$	7.02×10^{-14}
16	$CFU_j + HO_{2aq} \rightarrow CFU_j$	8.48×10^{-10}
17	$CFU_j + NO_{aq} \rightarrow CFU_j$	4.00×10^{-9}
18	$CFU_j + NO^-_{2aq} \rightarrow CFU_j + e_{aq}$	8.40×10^{-14}
19	$CFU_j + NO^-_{3aq} \rightarrow CFU_j + e_{aq}$	8.40×10^{-14}
20	$CFU_j + ONOO^-_{aq} \rightarrow CFU_j + e_{aq}$	8.40×10^{-14}
21	$CFU_k + O_{aq} \rightarrow CFU_k$	2.52×10^{-12}
22	$CFU_k + O^-_{aq} \rightarrow CFU_k + e_{aq}$	2.52×10^{-17}
23	$CFU_k + OH_{aq} \rightarrow CFU_k$	2.52×10^{-14}
24	$CFU_k + OH^-_{aq} \rightarrow CFU_k + e_{aq}$	2.87×10^{-17}
25	$CFU_k + H_2O_{2aq} \rightarrow CFU_k + H_2O_{aq}$	7.02×10^{-17}
26	$CFU_k + HO_{2aq} \rightarrow CFU_k$	8.48×10^{-13}
27	$CFU_k + NO_{aq} \rightarrow CFU_k$	4.00×10^{-10}
28	$CFU_k + NO^-_{2aq} \rightarrow CFU_k + e_{aq}$	8.40×10^{-12}
29	$CFU_k + NO^-_{3aq} \rightarrow CFU_k + e_{aq}$	8.40×10^{-12}
30	$CFU_k + ONOO^-_{aq} \rightarrow CFU_k + e_{aq}$	8.40×10^{-12}
31	$CFU_l + O_{aq} \rightarrow CFU_l$	2.52×10^{-9}
32	$CFU_l + O^-_{aq} \rightarrow CFU_l + e_{aq}$	2.52×10^{-15}
33	$CFU_l + OH_{aq} \rightarrow CFU_l$	2.52×10^{-13}
34	$CFU_l + OH^-_{aq} \rightarrow CFU_l + e_{aq}$	2.87×10^{-15}
35	$CFU_l + H_2O_{2aq} \rightarrow CFU_l + H_2O_{aq}$	7.02×10^{-14}
36	$CFU_l + HO_{2aq} \rightarrow CFU_l$	8.48×10^{-13}
37	$CFU_l + NO_{aq} \rightarrow CFU_l$	4.00×10^{-11}
38	$CFU_l + NO^-_{2aq} \rightarrow CFU_l + e_{aq}$	8.40×10^{-13}
39	$CFU_l + NO^-_{3aq} \rightarrow CFU_l + e_{aq}$	8.40×10^{-13}
40	$CFU_l + ONOO^-_{aq} \rightarrow CFU_l + e_{aq}$	8.40×10^{-13}
41	$CFU_m + O_{aq} \rightarrow CFU_m$	2.52×10^{-10}
42	$CFU_m + O^-_{aq} \rightarrow CFU_m + e_{aq}$	2.52×10^{-16}
43	$CFU_m + OH_{aq} \rightarrow CFU_m$	2.52×10^{-14}
44	$CFU_m + OH^-_{aq} \rightarrow CFU_m + e_{aq}$	2.87×10^{-16}
45	$CFU_m + H_2O_{2aq} \rightarrow CFU_m + H_2O_{aq}$	7.02×10^{-15}
46	$CFU_m + HO_{2aq} \rightarrow CFU_m$	8.48×10^{-13}
47	$CFU_m + NO_{aq} \rightarrow CFU_m$	4.00×10^{-12}
48	$CFU_m + NO^-_{2aq} \rightarrow CFU_m + e_{aq}$	8.40×10^{-14}
49	$CFU_m + NO^-_{3aq} \rightarrow CFU_m + e_{aq}$	8.40×10^{-14}
50	$CFU_m + ONOO^-_{aq} \rightarrow CFU_m + e_{aq}$	8.40×10^{-14}
51	$CFU_n + O_{aq} \rightarrow CFU_n$	2.52×10^{-11}
52	$CFU_n + O^-_{aq} \rightarrow CFU_n + e_{aq}$	2.52×10^{-17}
53	$CFU_n + OH_{aq} \rightarrow CFU_n$	2.52×10^{-15}
54	$CFU_n + OH^-_{aq} \rightarrow CFU_n + e_{aq}$	2.87×10^{-17}
55	$CFU_n + H_2O_{2aq} \rightarrow CFU_n + H_2O_{aq}$	7.02×10^{-16}

(Continued.)

Table 1. (Continued.)

56	$CFU_n + HO_{2aq} \rightarrow CFU_n$	8.48×10^{-14}
57	$CFU_n + NO_{aq} \rightarrow CFU_n$	4.00×10^{-12}
58	$CFU_n + NO^-_{2aq} \rightarrow CFU_n + e_{aq}$	8.40×10^{-17}
59	$CFU_n + NO^-_{3aq} \rightarrow CFU_n + e_{aq}$	8.40×10^{-17}
60	$CFU_n + ONOO^-_{aq} \rightarrow CFU_n + e_{aq}$	8.40×10^{-17}
71	$CFU_x + O_{aq} \rightarrow CFU_x$	2.52×10^{-13}
72	$CFU_x + O^-_{aq} \rightarrow CFU_x + e_{aq}$	2.52×10^{-18}
73	$CFU_x + OH_{aq} \rightarrow CFU_x$	2.52×10^{-15}
74	$CFU_x + OH^-_{aq} \rightarrow CFU_x + e_{aq}$	2.87×10^{-18}
75	$CFU_x + H_2O_{2aq} \rightarrow CFU_x + H_2O_{aq}$	7.02×10^{-18}
76	$CFU_x + HO_{2aq} \rightarrow CFU_x$	8.48×10^{-14}
77	$CFU_x + NO_{aq} \rightarrow CFU_x$	4.00×10^{-13}
78	$CFU_x + NO^-_{2aq} \rightarrow CFU_x + e_{aq}$	8.40×10^{-18}
79	$CFU_x + NO^-_{3aq} \rightarrow CFU_x + e_{aq}$	8.40×10^{-18}
80	$CFU_x + ONOO^-_{aq} \rightarrow CFU_x + e_{aq}$	8.40×10^{-18}

(a) $0 \leqslant i \leqslant 20$
(b) $0 \leqslant j \leqslant 3$
(c) $4 \leqslant k \leqslant 7$
(d) $8 \leqslant l \leqslant 11$
(e) $12 \leqslant m \leqslant 15$
(f) $16 \leqslant n \leqslant 19$
(g) $x = 20$.

abstraction were considered, as the hydrogen abstraction step was determined to be the rate limiting step in the modification of the cysteine molecule. Based on the cysteine mechanism, O_{aq}, O_{aq}^-, OH_{aq}, OH_{aq}^-, HO_{2aq}, and H_2O_{2aq} are the ROS allowed to interact with the cell in solution and result in damage. Reactions with NO_{aq}, NO_{2aq}^-, NO_{3aq}^-, and $ONOO_{aq}^-$ were also included as these species have been shown to be important for wound healing and for bacterial inactivation [33, 34]. Rates for cell interaction with RONS were adjusted from those published in [26]. to be consistent with timescales for achieving bacterial cell inactivation reported in the literature. In particular, studies by Van Gils *et al* [15] and Chandana *et al* [16] were most influential in determining rates of reactions and time to cell killing.

In practice, cells are plated in solution containing cell media or broth which provides key nutrients for keeping cells alive. Cell media or broth consists of vitamins, proteins, and other organic matter that can scavenge or produce RONS. In the model, the growth medium is not accounted for as a separate species. Instead, we consider one colony forming unit (CFU) to approximate a cell plus its associated media.

In the hierarchical cell reaction mechanism, an individual cell undergoes a series of sequential reactions with RONS that progressively damage the cell. The health of the cell is classified by how many sequential interactions it has undergone. Based on the typical size and surface site density of a planktonic cell such as *P. aeruginosa*, we assume our idealized cell to have 10^8 reaction sites. A cell is classified as being no longer viable when 10% of those sites have undergone reaction with RONS, or 10^7 discrete reactions have taken place. That is C_0 (a healthy cell) reacts with a RONS species to become a damaged cell C_1. The now damaged cell C_1 reacts with a RONS species to become a damaged cell C_2. For a real cell, this sequence would occur 10^7 times until the cell is classified as being dead. As it is impractical to track the 10^7 discrete events for one individual cell that are required to declare the cell dead, 20 sequential generations of increasingly damaged cells were tracked. The 20th generation of the cell is considered dead. The consumption of RONS is accelerated by the ratio of the number of discrete reactions required to kill a cell (10^7) to the number of generations of the model cells (20) to approximate reaction rates with real cells. A set of 'ghost' reactions in which consumption of RONS does not result in cell damage are included to reflect the actual RONS consumption. Rates of RONS consumption are assumed to be slower for cells that are more damaged, as the number of reactive sites decreases. An example of the populations of the cell death model as a function of treatment time, including all 20 generations of sequentially damaged cells is shown in figure 3(a). An initial CFU density of 1×10^7 cm^{-3} was chosen to be consistent with the initial concentration of CFUs that might be present in a cell culture. These results are for the base case plasma treatment with a remote, non-touching plasma source, and will be discussed in more detail below.

In experiments, following plasma treatment some fraction of damaged cells can recover and become healthy cells, while a fraction of treated, but still live cells is irreparably damaged and will eventually die. In this work, the successive cell generations of damaged cells are divided into three groups. The first group (generation C_0 to generation C_6) is classified as being healthy. The second group (generation C_7 to generation C_{13}) is classified as being sick, and the last third (generation C_{14} to generation C_{20}) are cells that will die in the short term. Cells C_{20} are immediately dead. (See figure 3(b)).

Most experimental measurements of cell viability occur over the long term by re-plating the CFUs and assessing reproduction of those cells. Healthy cells reproduce. Over this

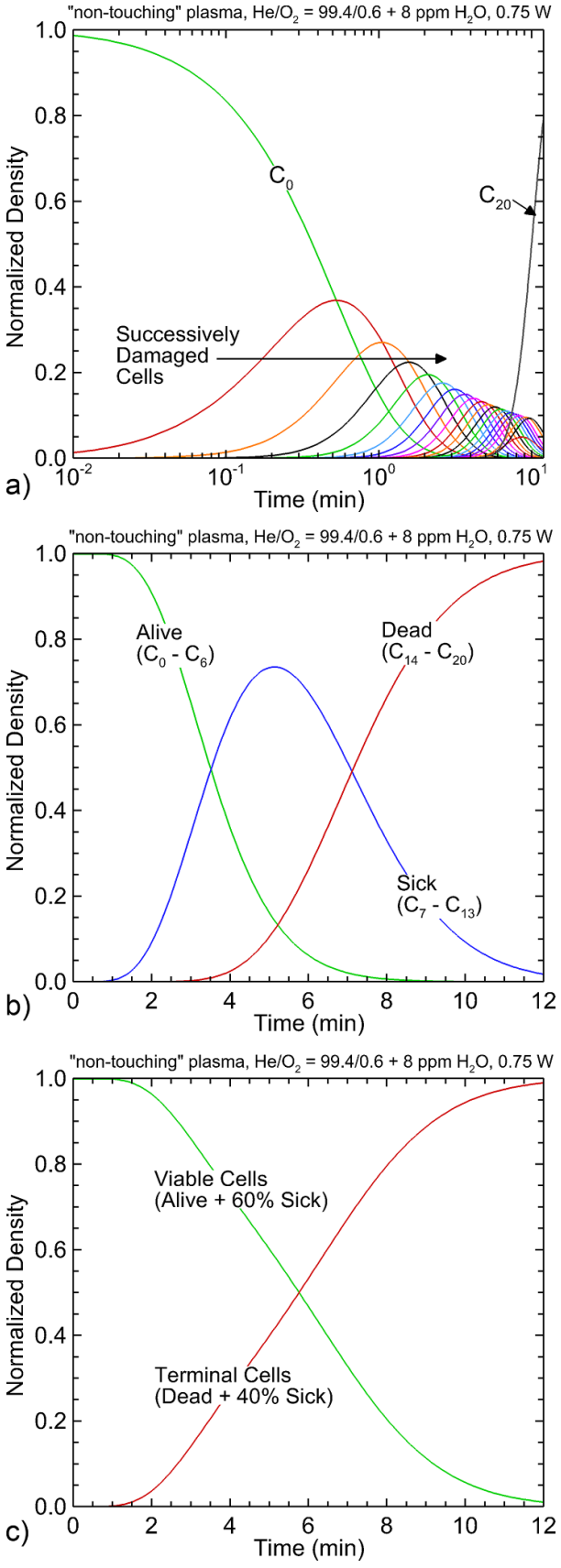

Figure 3. Results from the cell death model including (a) 20 generations of damaged CFU, (b) division of generations into alive, sick, and dead, and (c) estimate of viable ir terminal cell populations. Initial CFU concentration was 10^7 cm^{-3}.

longer assessment period, we assume that the heavily damaged cells die as do a fraction of the sick cells. To achieve consistency with times for cell death reported in the literature, we estimated that 60% of the sick population will recover and classified this population as being alive, while 40% of the sick population will not recover and is classified as dead. In the discussion that follows we classify as being *viable* the healthy population plus 60% of the sick population. We classify as being *terminal* the heavily damaged and dead population plus 40% of the sick population (figure 3(c). The estimation that 60% of the sick population recovers while only 40% is terminal is intended to account for long time periods between treatment and measurement that often occur under experimental conditions in which the healthy cell population may reproduce.

3. Base case plasma and liquid properties

The base case uses an indirect (non-touching) source patterned after the COST-jet (figure 1(a)). The plasma chamber consists of two 1 mm wide by 3 cm long rectangular electrodes spaced 1 mm apart. One electrode is powered by 750 mW of constant RF power while the other electrode is grounded. Inlet gases consist of 1000 sccm of a $He/O_2 = 99.4/0.6$ mixture containing 8 ppm of water impurity flowing from the top of the reactor and plasma is generated between the two electrodes. The plasma is assumed to be uniform over the 1 mm^2 cross sectional-area. The outlet of the plasma source is at 3 cm where plasma effluent flows out of the source and mixes with ambient humid air ($N_2/O_2/H_2O = 78/20/2$). The effluent is exposed to the ambient air over a gap distance of 4 mm before coming into contact with the liquid surface. The liquid surface is exposed to the plasma effluent for up to 12 min. The treated liquid is 1 ml of water. An initial concentration of CFU in the water is not included in the base case so that RONS delivery to the liquid can be evaluated independently of the presence of organic material.

The gas phase production of selected RONS in the plasma source and in the gap between the reactor outlet and liquid surface are shown in figure 4. The model predicts an electron density of 6.8×10^{10} cm^{-3} in the plasma source which is consistent with experimental measurements of the helium COST-jet, which are on the order of a few times 10^{10} cm^{-3} when the power is a few hundred milliwatts to a few watts [13]. Production of atomic O (7.9×10^{15} cm^{-3}) is also consistent with literature values, which is reported to be on the order of a few times 10^{15} cm^{-3} [35].

ROS including HO_2, OH and H_2O_2 are formed in the powered region of the plasma source as a result of the water impurity. Water is dissociated by electron impact and heavy particle dissociative excitation transfer (DET) to form OH and HO_2. H_2O_2 is formed through reaction of H_2O dissociation products.

$$e + H_2O \rightarrow OH + H + e \quad (1)$$

$$He^* + H_2O \rightarrow He + OH^+ + H + e \quad (2)$$

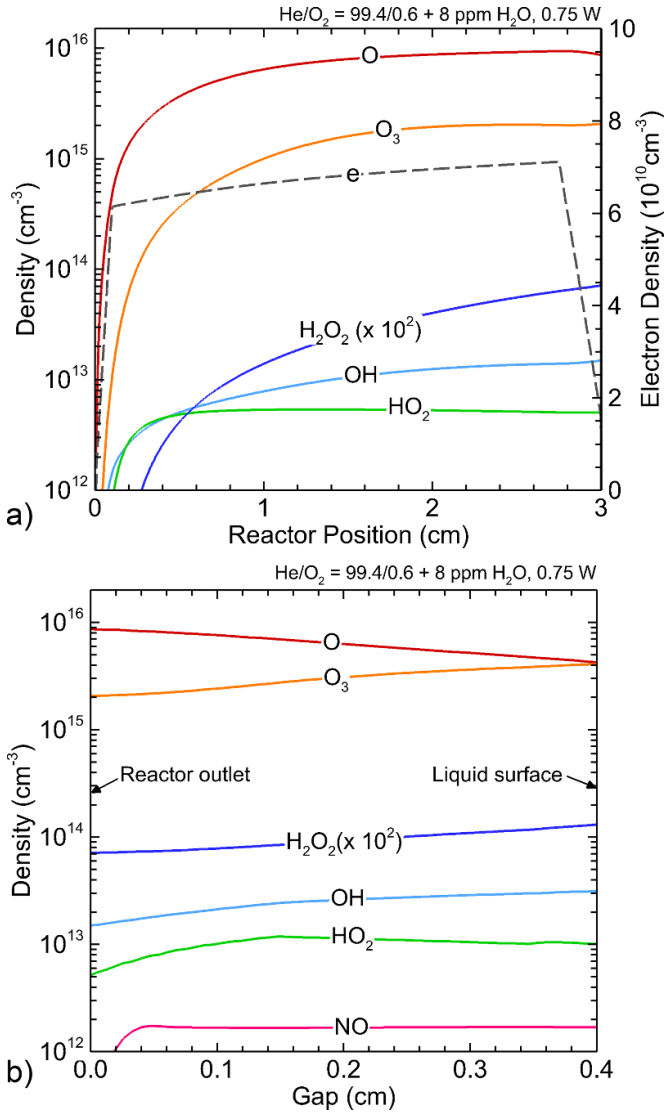

Figure 4. Gas-phase species production for the indirect plasma source (a) in the reactor and (b) in the air gap between the reactor outlet and liquid surface.

$$He_2^* + H_2O \rightarrow 2He + OH^+ + H + e \quad (3)$$

$$He^* + H_2O \rightarrow He + OH^* + H \quad (4)$$

$$He_2^* + H_2O \rightarrow 2He + OH^* + H \quad (5)$$

$$OH + OH \rightarrow H_2O_2 \quad (6)$$

$$HO_2 + H_2O \rightarrow H_2O_2 + OH. \quad (7)$$

As the plasma effluent exits the powered region and comes into contact with ambient air, electron impact ionization and excitation essentially cease. There is some small production of O, H and OH due to due to dissociative recombination of O_2^+ and H_2O^+, but this additional contribution is small compared to the O, H and OH already contained in the flow. NO_x species are then formed in the air gap. NO_x is formed through reaction of nitrogen dissociation products and plasma produced ROS. However, since no N-containing species flowed through the plasma, the production of RNS is nominal. RONS produced in

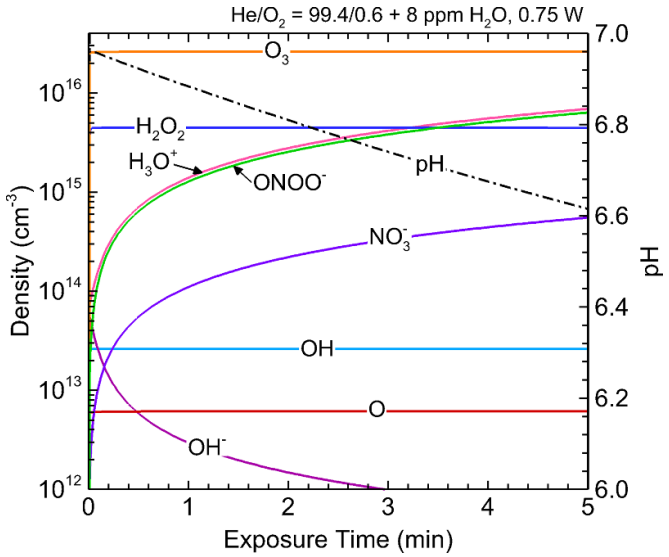

Figure 5. Liquid species densities and pH as a function of plasma exposure time using the indirect plasma source. There are no CFU in the liquid.

the powered region and in the air gap impinge upon the liquid surface and solvate into the liquid as described above. The production of select liquid-phase RONS are shown in figure 5 as a function of plasma exposure time.

Species with moderate Henry's law coefficients (e.g. O and OH) solvate and quickly come to equilibrium, whereas species with low Henry's law coefficients (e.g. NO, O_3) solvate less readily. Production of long-lived species such as H_2O_{2aq} and O_{3aq} is due partially to solvation and partially to liquid-phase reaction of solvated ROS.

$$O_{aq} + O_{2aq} \rightarrow O_{3aq} \quad (8)$$

$$HO_{2aq} + HO_{2aq} \rightarrow H_2O_{2aq} + O_{2aq} \quad (9)$$

$$OH_{aq} + OH_{aq} \rightarrow H_2O_{2aq}. \quad (10)$$

O_{3aq} (2.5×10^{16} cm^{-3}) and H_2O_{2aq} (4.5×10^{15} cm^{-3}) are the most abundant RONS produced in the liquid under these conditions at early treatment times. At later treatment times, reactions of solvated RNS with ROS contribute to an increase in peroxynitrite ($ONOO_{aq}^-$) and nitrate (NO_{3aq}^-). Peroxynitrite ($ONOO_{aq}^-$) is formed as a product of $O_{2\ aq}^-$ and NO_{aq}.

$$O_{2aq}^- + NO_{aq} \rightarrow ONOO_{aq}^-. \quad (11)$$

The $ONOO_{aq}^-$ concentration increases relative to H_2O_{2aq} concentration, and exceeds the concentration of H_2O_{2aq} after about 3.5 min of liquid exposure to the plasma effluent. This long time for buildup of the long lived $ONOO_{aq}^-$ is due to the low plasma production rate of RNS. The efficiency of the plasma to preferentially produce some RONS over others contributes to differences in times to achieve bacterial inactivation, as will be discussed in the following section.

The pH of the solution is also shown in figure 5. The pH decreases from 7 to about 6.6 over the first five minutes of

exposure time, indicating only mild acidification. This acidification can be attributed to the delivery of HNO_x to the liquid surface. $HNO_{x,aq}$ hydrolyzes in solution to produce $H_3O^+{}_{aq}$.

$$HNO_{xaq} + H_2O_{aq} \rightarrow H_3O^+_{aq} + NO^-_{xaq}. \quad (12)$$

The moderate decrease in pH results from the low flux of HNO_x onto the surface of the liquid for remote plasma sources. In the absence of nitrogen containing species flowing through the plasma, production of HNO_x occurs only in the air gap between the plasma source and the liquid.

4. Onset to cell death

The base case for assessing the onset of cell death is the $He/O_2 = 99.4/0.6$ gas mixtures whose plasma activated gas phase and liquid phase densities were discussed in the prior section. Cell viability curves for the He/O_2 base case are shown in figure 3 for an initial CFU concentration of 1×10^7 cm^{-3}. Cell killing does not begin immediately. There is a delayed onset to cell killing that corresponds to the time for RNS species such as $ONOO^-_{aq}$ and NO^-_{3aq} to begin to approach their saturation limit in solution (a little over 1 min). Nearly 100% of the CFU are classified as being alive for over 1 min of exposure time (figure 3(b). It then follows that the mechanism for cell death is most sensitive to the rates chosen for reactions with RNS species (reactions 7-10 in table 1). Increases in the rate coefficients for RNS reactions with CFUs resulted in times to cell death that were too short for non-touching configurations. Using the classification scheme described above, 50% of the cells are viable after 6 min of exposure and 50% are terminal. After 12 min of exposure, 99% of cells are classified as terminal.

4.1. Cell killing as a function of inlet gas composition

Changing the inlet plasma gas composition is a direct method to alter the composition of RONS interacting with the target and can be valuable for isolating the effects of specific RONS on cell death. Often, it is impractical to greatly alter the plasma gas composition experimentally, as small changes to the device configuration may, for example, alter plasma impedance and power matching. Parametric studies on gas mixtures using models can provide guidance for designing or optimizing experimental devices.

Cell viability after 12 min of plasma treatment time was evaluated using five inlet gas compositions: He, $He/O_2 = 99.4/0.6$, $Ar/O_2 = 99.4/0.6$, $He/N_2/O_2 = 99/0.8/0.2$, $Ar/N_2/O_2 = 99/0.8/0.2$. All compositions consisting of one or two gasses include a water impurity of 8 ppm. The tri-gas mixtures include a water impurity of 25 ppm. The choice of how much water impurity to include was based on ongoing modeling efforts for matching OH and H_2O_2 production in the COST-jet using He, He/O_2, and $He/N_2/O_2$ mixtures. The power was held constant at 750 mW for all gas compositions. The gap between the reactor outlet and the liquid surface was 4 mm and the initial CFU concentration was 1×10^7 cm^{-3}. CFU viability for all gas compositions over the 12 minute treatment period is shown in figure 6(a)

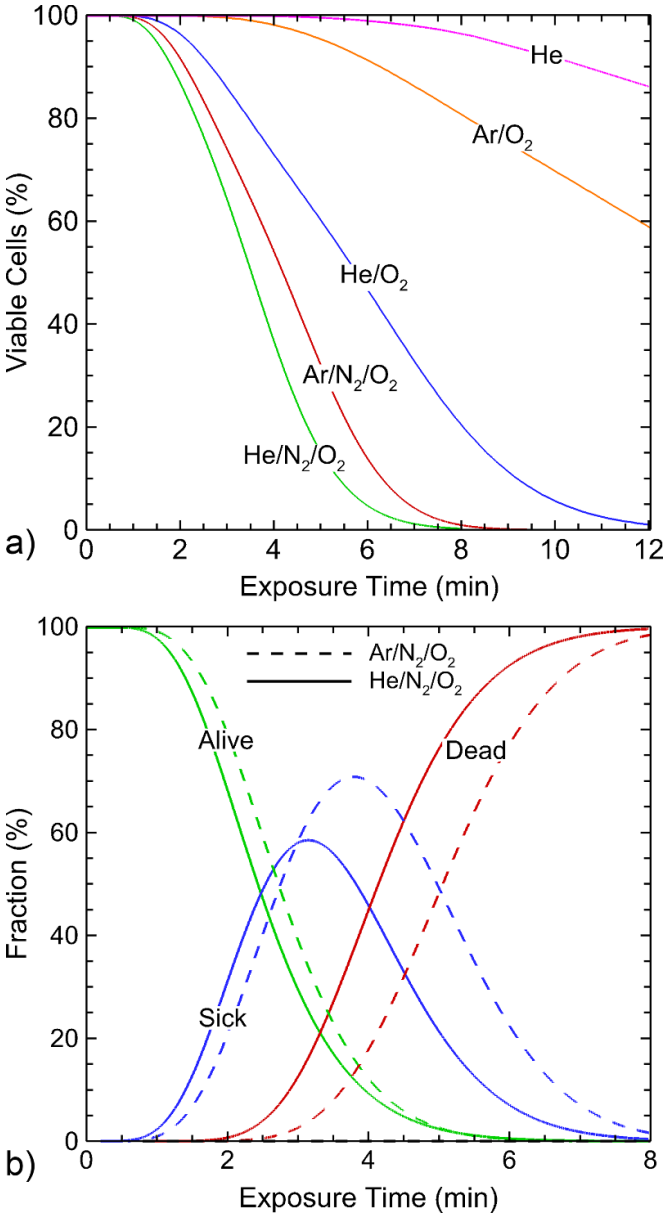

Figure 6. Cell viability over time for different inlet plasma gas compositions using the indirect plasma source: (a) He, $Ar/O_2 = 99.4/0.6$, $He/O_2 = 99.4/0.6$, $Ar/N_2/O_2 = 99/0.8/0.2$, $He/N_2/O_2 = 99/0.8/0.2$ and (b) fraction of viable, damaged, and terminal cells for the two tri-gas compositions.

Based on the hierarchal cell death model, for otherwise constant conditions, the tri-gas mixtures are the most efficient at cell killing, with nearly all cells killed after 8 min of treatment time. The cases in which O_2 (with H_2O impurity) was the only additive required an additional 4 min (He/O_2) or more (Ar/O_2) to produce similar reductions in viability. These results are consistent with those reported in the literature for a similar

plasma configuration. Chandana *et al* changed the gas composition in a touching APPJ to treat *E. Coli* under wet conditions [16]. They found that the addition of air as an impurity in both helium and argon plasmas reduced cell viability more efficiently than air, argon, or helium only plasmas. The effectiveness of the tri-gas cases can be attributed to the production of NO_x species in the plasma. NO_x delivery to the liquid results in formation of HNO_{xaq} which hydrolyzes to form $H_3O_{aq}^+$ and NO_{xaq}^- and lowers the pH of the solution.

$$NO_{xaq} + H_2O_{aq} \rightarrow HNO_{xaq} + OH_{aq} \quad (13)$$

$$HNO_{xaq} + H_2O_{aq} \rightarrow H_3O_{aq}^+ + NO_{xaq}^-. \quad (14)$$

Common bacteria such as *P. aeruginosa* and *E. Coli* are viable over a wide range of pH, and so the decrease in solution pH alone cannot explain the efficiency of nitrogen-containing plasmas for cell killing [36, 37]. However, the RNS NO_{2aq}^-, NO_{3aq}^-, $ONOO_{aq}^-$ are able to damage the CFU in our mechanism. Studies suggest that plasma-produced H_2O_{2aq} works in synergy with NO_{xaq}, in part via the formation of $ONOO_{aq}^-$, to increase the efficiency of cell killing [33]. It then follows that $He/N_2/O_2$ mixtures would be more efficient at cell killing than $Ar/N_2/O_2$ mixtures for our conditions, as the helium mixture produces double the gas-phase RNS than the argon mixture. For example, the density of NO delivered to the liquid surface is 5.9×10^{13} cm^{-3} for the helium mixture while 3×10^{13} cm^{-3} NO is delivered to the liquid surface for the argon mixture. These RNS solvate into the liquid and contribute to the formation of NO_{xaq}^- and $ONOO_{aq}^-$, which then damage the cells. The fractions of cells that are alive, sick, or dead for the $He/N_2/O_2$ and $Ar/N_2/O_2$ mixtures are shown in figure 6(b). Onset to cell death requires nearly one more minute of plasma exposure with the argon mixture compared to the He mixture, which is a direct consequence of the lower RNS production in the argon mixture.

The mixtures that contain only O_2 also produce cell killing, though these mixtures are less efficient at cell killing than those containing O_2 and N_2. For gas mixtures containing only rare gas and oxygen, NO_x species are only formed in significant amounts in the gap between the reactor outlet and the liquid surface as plasma-produced radicals react with N_2 in the air. Little NO_x is produced for these conditions as there is little direct dissociation of N_2 by electron impact or DET. Therefore, cell killing is largely due to ROS in these cases. More OH and H_2O_2 are delivered to the liquid surface in the argon-oxygen mixture than in the helium-oxygen mixture (1.7×10^{13} cm^{-3} OH and 2.8×10^{12} cm^{-3} H_2O_2 in argon; 1.1×10^{13} cm^{-3} OH and 3.6×10^{11} H_2O_2 in helium). DET from the argon metastable is more efficient at dissociating water than the helium metastable [38, 39].

More O_3 is also formed in the argon mixture compared to the He mixtures (1.5×10^{16} cm^{-3} in argon, 1.8×10^{15} cm^{-3} in helium). However, in the hierarchal cell death mechanism, O_3 does not directly impact cell viability and in previous studies was found to hinder modifications of organic molecules in solution [26]. The helium mixture is more efficient at producing atomic O, which both interacts directly with the CFU and contributes to the formation of other RONS in the air gap and in the liquid-phase after solvation. (8.2×10^{15} cm^{-3} O is delivered to the liquid surface in helium, 2.4×10^{15} cm^{-3} O is delivered to the liquid surface in argon.) The ability of the helium mixture to more efficiently dissociate O_2 to O, combined with the lower production of O_3, contributes to a higher rate of cell killing than in the argon mixture for this plasma source configuration, even though the gas-phase production of OH and H_2O_2 is less in the argon mixture.

Results from the model suggest that non-touching configurations that minimize O_3 production while maximizing O production (for example, plasma formed in He/O_2 rather than Ar/O_2) may be optimal for cell killing when nitrogen is not included in the gas mixture. Cell killing is most efficient when ROS and RNS are formed in the plasma (such as in the $He/N_2/O_2$ and $Ar/N_2/O_2$ mixtures) and can work synergistically to damage cells. The hierarchal model is able to capture trends for reduction in cell viability that are consistent with the findings produced by Chandana *et al* [16] when the inlet gas composition is changed.

4.2. Cell killing as a function of plasma source configuration

Cell viability for different gas mixtures was discussed for *non-touching* conditions. For these conditions, the plasma is well confined between the electrodes and does not extend downstream. The plasma produced reactants in the plume that reach the liquid consist dominantly of neutral species. The opposite extreme in plasma source design is a *touching* configuration, in which the active plasma extends from the plasma source to (and touches) the surface of the liquid. Investigations of cell viability for a *touching* source that is approximately based on the kINPen [4, 40] (figure 1(b)) were performed to compare to the *non-touching* configuration. The *touching* configuration consists of a 1 cm long plasma zone in the actual source with a plasma plume that extends beyond the source by 4 mm to touch the liquid. Of the 750 mW total power deposition, about 89% is deposited in the plasma source. The remainder of the power is expended in the gap, with the profile as a function of position shown in figure 7. The power is non-zero at the liquid surface.

Plasma forms inside the source and extends across the 4 mm air gap to impinge upon the liquid surface. Unlike in the non-touching configuration, the ambient air diffusing into the plume can participate in electron impact and ion collisional processes that can lead to higher production of RONS in the air gap. The production of select RONS in the air gap is shown in figure 7. For the same power deposition, the touching configuration is more effective overall at producing key cell killing RONS in the gas phase such as OH, H_2O_2 and NO. Densities of these species increase across the air gap in the touching case as a result of the power expended in the gap that allows for continued electron impact processes. In the non-touching case, the production of these species stagnates as reactive neutrals are consumed in reactions with the ambient air.

The density of H_2O_2 increases by nearly an order of magnitude in the air gap while the increase in OH and HO_2 is

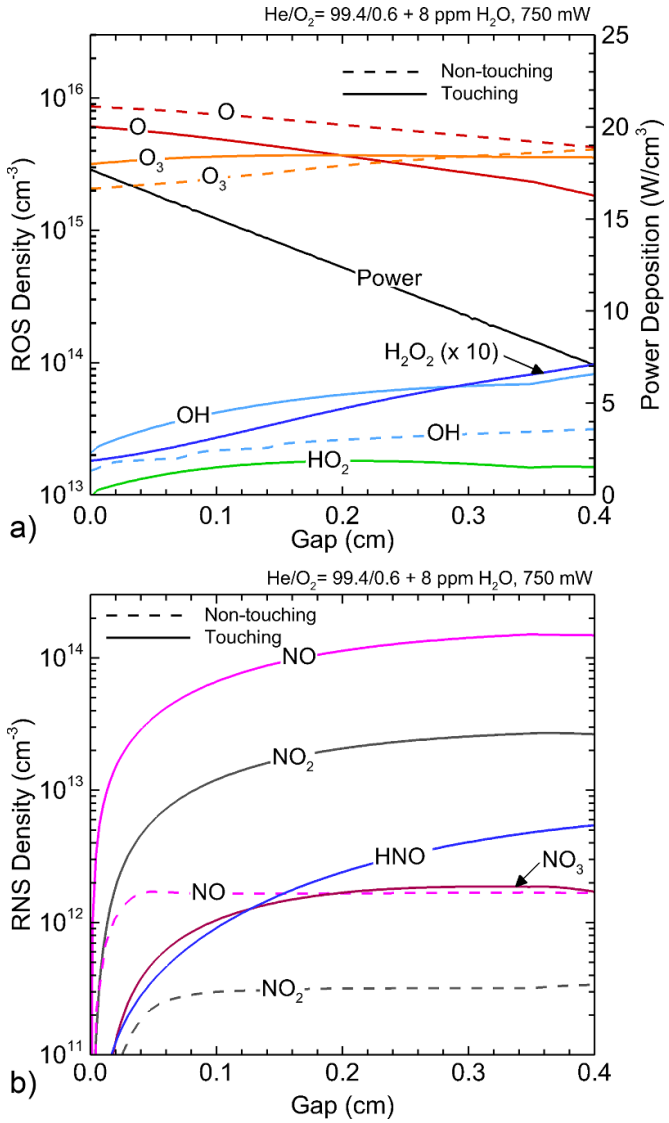

Figure 7. Reactive species density in the air gap for 'touching' and 'non-touching' plasma source configurations. (a) ROS and (b) RNS.

less pronounced (a few times the density at the exit of the plasma source). The densities at the surface of the liquid are 9.7×10^{12} cm^{-3} for H_2O_2, 8.2×10^{13} cm^{-3} for OH, and 1.6×10^{13} cm^{-3} for HO_2 in the touching configuration. These densities in the non-touching configuration are 1.3×10^{12} cm^{-3} for H_2O_2, 3.1×10^{13} cm^{-3} for OH, and 1.0×10^{13} for HO_2. In both configurations the density of O decreases across the air gap as three-body reactions involving O_2 convert O to O_3. In the touching configuration, the density of O_3 increases in the air gap from 3.1×10^{15} cm^{-3} at the exit of the plasma source to about 3.6×10^{15} cm^{-3} at the liquid surface. This is a less pronounced increase than in the non-touching configuration where the density of O_3 is 2.0×10^{15} cm^{-3} at the reactor outlet and 4.1×10^{15} cm^{-3} at the liquid surface. In the touching configuration, O is more efficiently converted to NO_x products rather than O_3, as shown in figure 7(b). The touching plasma is able to deliver 1.5×10^{14} cm^{-3} NO, 2.7×10^{13} cm^{-3} NO_2, 1.7×10^{12} cm^{-3} NO_3, and 5.4×10^{12} cm^{-3} HNO to the liquid surface. The densities of these same species at the liquid surface in the non-touching configuration are two orders of magnitude lower. HNO_{aq} hydrolyzes to form $H_3O^+{}_{aq}$. The production of $H_3O^+{}_{aq}$ contributes to acidification of the solution. The final pH of the solution is around 3 in the touching configuration and 4.5 in the non-touching configuration.

The delivery of the fluxes of plasma produced species to the liquid integrated over time, or the fluence, aligns with the production of gas-phase species. Fluences are shown in figure 8. Higher gas-phase production and delivery to the surface of most RONS by the touching plasma generally leads to higher production of liquid-phase RONS than the non-touching plasma. RONS concentrations in the liquid as a result of the two plasma configurations are shown in figure 9.

Both plasma configurations generate similar concentrations of H_2O_{2aq} and OH_{aq}, however, the touching configuration generates significantly more HO_{2aq}. The touching plasma produces 3.8×10^{15} cm^{-3} H_2O_{2aq}, 1.8×10^{13} cm^{-3} OH_{aq}, and 5.7×10^{13} cm^{-3} HO_{2aq} while the non-touching plasma generates 4.5×10^{15} cm^{-3} H_2O_{2aq}, 2.6×10^{13} cm^{-3} OH_{aq}, and 2.4×10^{11} cm^{-3} HO_{2aq}. The high generation rate of HO_{2aq} for the touching source is largely due to the high rate of generation of HNO and NO_3 in the air gap. These species then solvate into the liquid. NO_{3aq} reacts with H_2O_{2aq} and HNO_{aq} reacts with O_{2aq} to generate HO_{2aq} in solution.

$$H_2O_{2aq} + NO_{3aq} + H_2O_{aq} \rightarrow HO_{2aq} + NO^-_{3aq} + H_3O^+_{aq} \quad (15)$$

$$HNO_{aq} + O_{2aq} \rightarrow HO_{2aq} + NO_{aq}. \quad (16)$$

The reaction with NO_{3aq} results in a higher rate of in-solution consumption of H_2O_{2aq} than in the non-touching configuration. Higher generation and delivery of HNO_x and other RNS by the touching plasma leads to nearly two orders of magnitude higher production of aqueous RNS than the non-touching plasma. The touching configuration produces 1.9×10^{12} cm^{-3} NO_{aq}, 4.5×10^{12} cm^{-3} NO_{2aq}, 9.5×10^{12} cm^{-3} $NO_{2aq}{}^-$, 1.1×10^{17} cm^{-3} $NO_{3aq}{}^-$, and 4.9×10^{17} cm^{-3} $ONOO_{aq}{}^-$.

The combined effects of higher HO_{2aq} and aqueous RNS generation contributes to nearly two times faster cell killing by the touching plasma. Viability as a function of treatment time for an initial density of 1×10^7 cm^{-3} CFU is shown in figure 10. The touching plasma kills $> 99.9\%$ CFUs after 6 min of exposure while the non-touching plasma requires nearly 12 min to achieve the same result. Time for cell killing is consistent with reports by Van Gils *et al*, Chandana *et al* and Deng *et al* for time to bacterial inactivation for similar touching and non-touching systems [15–17].

Similar to the non-touching cases where higher gas-phase production of RNS led to more efficient cell killing, the improved killing efficiency of the touching plasma is due in part to its enhanced ability to produce RNS in the air gap. However, this is likely not the only explanation for its experimentally observed higher efficiency. For example, it has been shown that the electrical properties of touching plasmas may

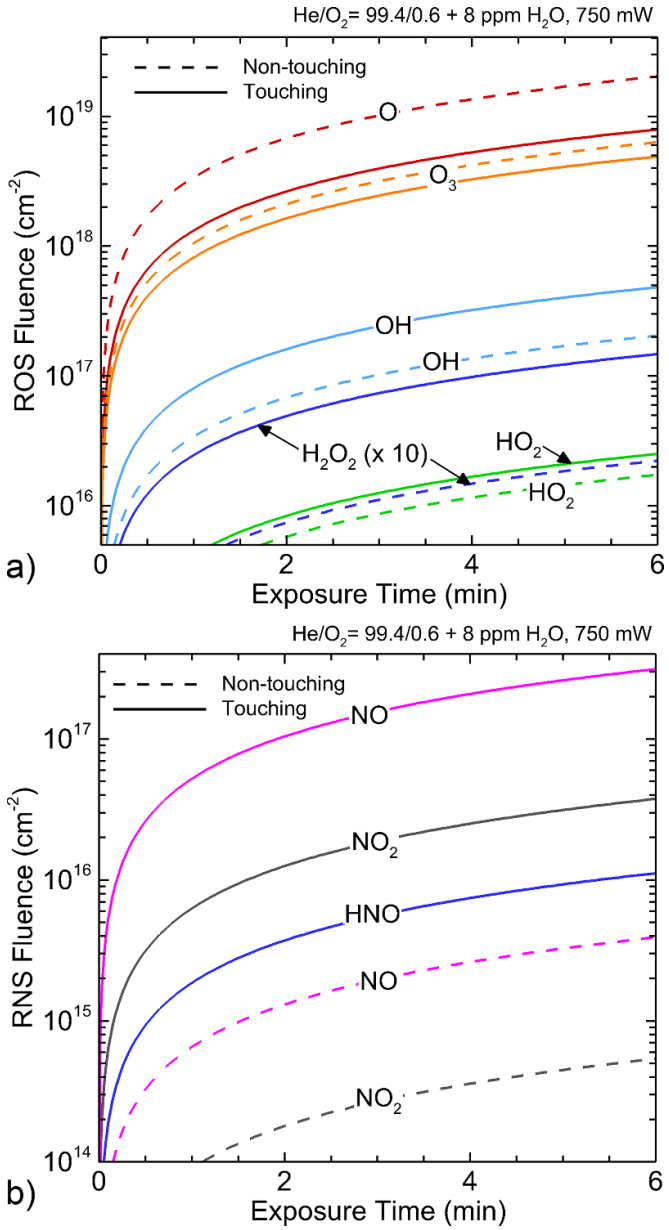

Figure 8. Comparison of fluence of gas-phase (a) ROS and (b) RNS to the liquid surface over time in touching and non-touching configurations.

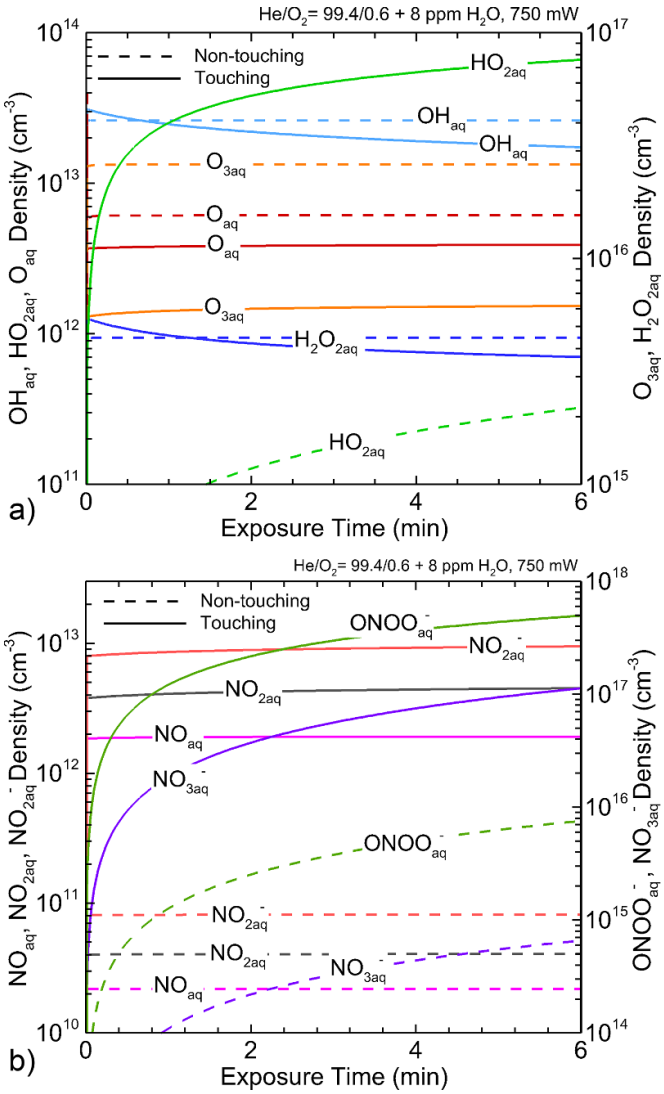

Figure 9. Densities of liquid-phase (a) ROS and (b) RNS over time for touching and non-touching configurations.

interrupt cellular redox pathways, in turn affecting the electrical properties of the biological target and creating a feedback loop between the plasma and the cells [41]. While cell or liquid charging is beyond the scope of the current investigation, the effects that the biological target has on the plasma (e.g. electrical properties, RONS production by the target) should be evaluated and considered in future models for holistic plasma device design.

4.3. Cell killing as a function of the air gap for the touching plasma

Production of RNS is a direct consequence of air entrainment in the air gap for APPJ configurations where nitrogen is not included in the gas inlet. Touching configurations are more effective at producing RNS in the air gap, as plasma extends into the air gap and allows for continued production of reactive species by electron impact processes. However, more air entrainment does not necessarily correspond to more effective bacterial inactivation. To investigate these issues, the length of the air gap in the model for the touching plasma was varied between 1 mm and 10 mm. The spatial slope of the power in the gap as shown in figure 7(a) was held constant, so shorter gaps had larger power at the surface of the liquid. Air entrainment was also adjusted between 2% of the gas inlet flow for a 1 mm gap and 9.5% for a 10 mm gap. The gas inlet flow conditions ($He/O_2 = 99.4/0.6 + 8$ ppm H_2O, 1010 sccm) and total power deposition (750 mW) were held constant. The reactor geometry is the same as discussed in the previous section and the initial CFU concentration was 10^7 cm^{-3}.

Cell viability over a 12 min plasma exposure time for air gaps between 1 mm and 10 mm is shown in figure 11. The viability curve for the non-touching base case (air

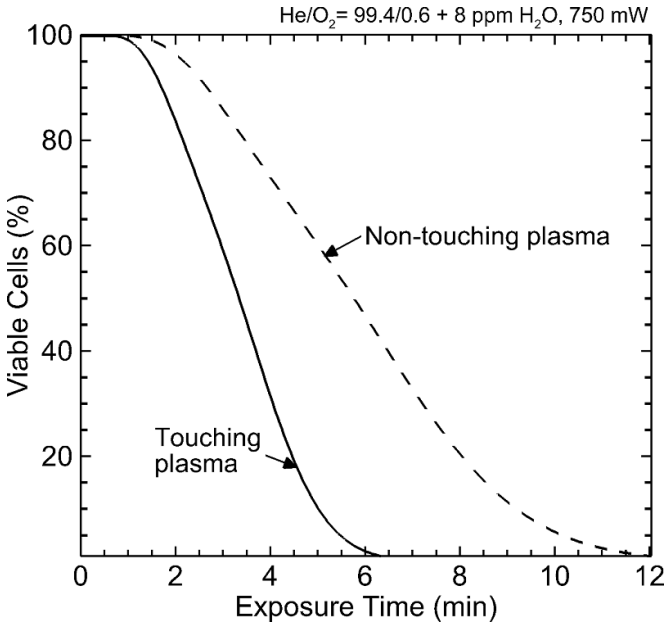

Figure 10. CFU viability as a function of plasma exposure time for two plasma source configurations (touching and non-touching).

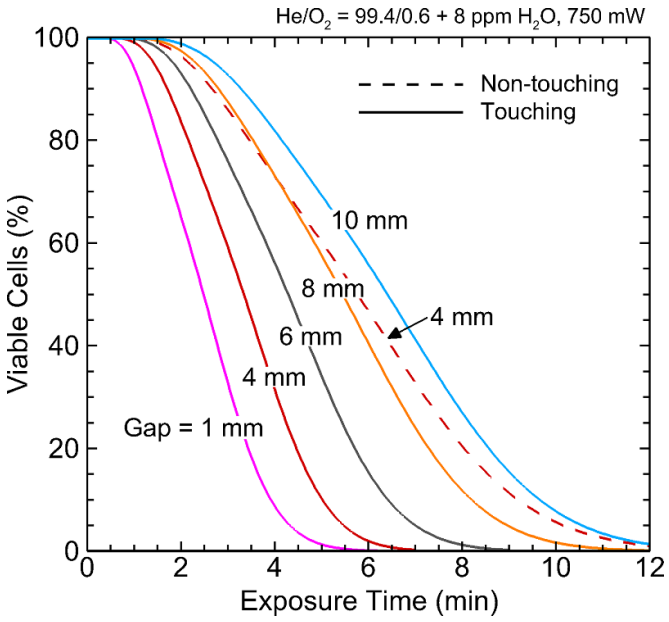

Figure 11. CFU viability as a function of plasma source distance from the liquid surface (air gap).

gap = 4 mm) is also shown for comparison. The touching plasma is effective for bacterial inactivation when the air gap is between 1 mm and 10 mm with a decreasing efficiency for increasing air gap. The time to achieve 1% viability is about 5.5 min with a 1 mm gap and 12.5 min with the 10 mm gap. Fluxes of gas-phase RONS to the liquid surface are shown in figure 12(a). The time to reduce cell viability by 80% as a function of air gap is shown in figure 12(b). The corresponding concentrations of select liquid-phase ROS and RNS produced by these fluxes at the time when CFU viability has been reduced by 80% are shown in figure 13.

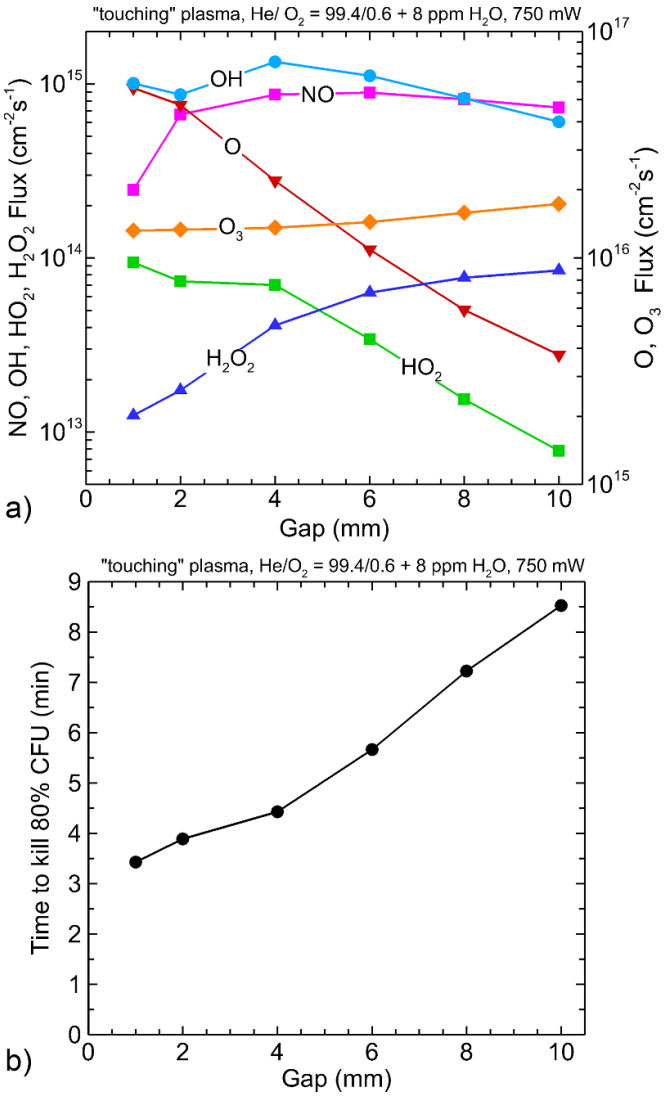

Figure 12. Reactant properties as a function of the air gap. (a) Gas-phase RONS fluxes to the liquid surface and (b) time required for fluxes to reduce CFU viability by 80%.

In general, smaller air gaps produce higher fluxes of gas-phase ROS and lower fluxes of gas-phase RNS to the liquid surface than larger air gaps. The exceptions are the fluxes of O_3 and H_2O_2. The 1 mm gap delivers fluxes of 1.3×10^{16} cm^{-2} s^{-1} O_3 and 1.2×10^{13} cm^{-2} s^{-1} H_2O_2 to the liquid surface while the 10 mm gap delivers fluxes of 1.7×10^{16} cm^{-2} s^{-1} O_3 and 8.5×10^{13} cm^{-2} s^{-1} H_2O_2. The flux of O_3 in the 10 mm gap is higher than in the non-touching base case (1.8×10^{13} cm^{-2} s^{-1}). As O_3 does not directly contribute to cell killing while consuming O (which does contribute to cell-killing), the high O_3 delivery to the liquid surface resulting from larger air gaps likely contributes to less efficient cell killing. The NO flux has the greatest increases between the 1 mm gap and the 2 mm gap before reaching a maximum in the 6 mm gap and decreasing gradually at larger gaps. The NO fluxes are 2.5×10^{14} cm^{-2} s^{-1} for the 1 mm gap, increasing to 8.9×10^{14} cm^{-2} s^{-1} for the 6 mm gap, and decreasing to 7.3×10^{14} cm^{-2} s^{-1} for the 10 mm gap. Although

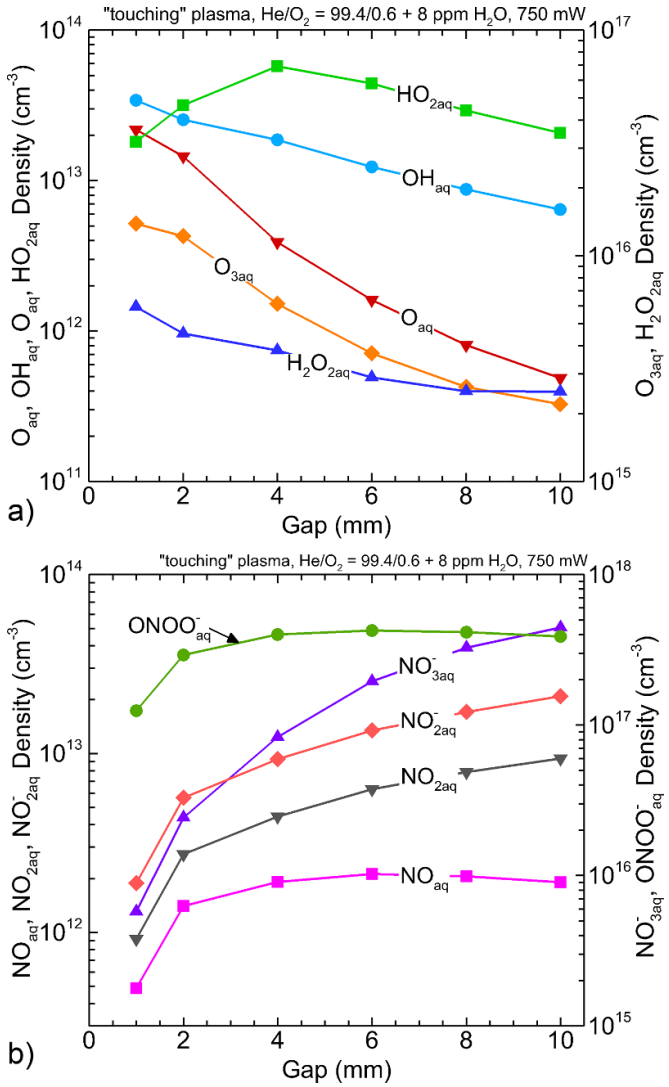

Figure 13. Liquid-phase (a) ROS and (b) RNS densities to achieve 80% reduction in CFU viability.

H_2O_2 delivery is greatest with the largest air gaps, the corresponding decrease in HO_2 (9.4×10^{13} cm^{-2} s^{-1} for 1 mm and 7.8×10^{12} cm^{-2} s^{-1} for 10 mm gap) and O delivery (5.6×10^{16} cm^{-2} s^{-1} for 1 mm and 3.7×10^{15} cm^{-2} s^{-1} for 10 mm) results in an overall lower production of liquid phase ROS and longer times to cell killing with the larger air gaps. The 1 mm air gap achieves 80% reduction in CFU viability 2.5 times faster than the 10 mm air gap as a consequence of these trends in fluxes of RONS in the air gap.

At the time of 80% cell killing, the NO_{xaq} concentrations are highest for larger gaps as a consequence of there being longer exposure times. There are densities of 4.9×10^{11} cm^{-3} NO_{aq}, 1.9×10^{12} cm^{-3} $NO_2^-{}_{aq}$, and 5.7×10^{15} cm^{-3} $NO_3^-{}_{aq}$ for a gap of 1 mm at the time of 80% cell killing—3.5 min. For a gap of 10 mm and killing time of 8.5 min, these concentrations are 1.9×10^{12} cm^{-3} NO_{aq}, 2×10^{13} cm^{-3} $NO_2^-{}_{aq}$, and 4.4×10^{17} cm^{-3} $NO_3^-{}_{aq}$. These higher concentrations of NO_{xaq} at the time of 80% cell killing are due in part to higher fluxes of H_2O_2. H_2O_2 solvates and produces $NO_3^-{}_{aq}$ through Reaction 14. Although the NO_{xq} concentrations increase with larger air gaps, the $ONOO^-_{aq}$ concentration at the time of 80% cell killing is nearly constant for air gaps between 4 mm and 10 mm (about 4×10^{17} cm^{-3}), which may indicate that this density of $ONOO^-_{aq}$ is critical for cell killing. Producing this concentration of $ONOO^-_{aq}$ requires an air gap large enough that air entrainment produces a sufficient RNS flux. $ONOO^-_{aq}$ is dominantly produced in the liquid by reactions between $O_2^-{}_{aq}$ and NO_{aq} (equation (11)). Smaller gaps can achieve the critical $ONOO^-_{aq}$ density at short times due to higher power at the liquid surface, which contributes to a higher flux of $O_2^-{}_{aq}$ onto the liquid surface. However, $ONOO^-_{aq}$ production is likely limited by the flux of NO, which does not change significantly when the air gap is between 4 mm and 10 mm.

Larger air gaps produce lower ROS fluxes and higher RNS fluxes onto the liquid surface. As a result, aqueous ROS concentrations at the time of 80% cell killing are lower with larger air gaps. The concentrations of ROS such as O_{aq} are diminished at larger air gaps as gas phase O is converted to O_3 or NO_x before reaching the liquid surface, while H_2O_{2aq} decreases at longer treatment times as it is consumed in reactions with NO_{xaq}. For example, when CFU viability has been reduced by 80%, there are densities of 2.2×10^{13} cm^{-3} O_{aq} and 2.6×10^{16} cm^{-3} H_2O_{2aq} for a gap of 1 mm. For a gap of 10 mm these concentrations are 4.9×10^{11} cm^{-3} O_{aq} and 4.3×10^{16} cm^{-3} H_2O_{2aq}. Lower ROS fluxes result in longer time to ROS accumulation to achieve critical densities for cell killing.

If RNS such as $ONOO^-_{aq}$ were solely responsible for cell killing, then smaller gaps (where fluxes of RNS are lower) should be less efficient at cell killing than larger gaps. Results indicate that a balance of ROS and RNS delivery is needed to maximize the efficiency of plasma systems for bacterial inactivation. Configurations (such as the non-touching plasma) that contribute primarily ROS fluxes and that produce liquid-phase ROS are not as effective in cell deactivation as systems that can produce both ROS and RNS in the liquid-phase. Configurations that maximize RNS fluxes to the liquid while minimizing ROS fluxes (such as the touching plasma with 10 mm air gap) are the least efficient at cell deactivation. Configurations that exclusively produce large densities of O_3 in the gas-phase are also not ideal. Results reinforce the importance of considering both ROS and RNS production (in both the gas and liquid phases) when designing devices for bacterial inactivation.

5. Concluding remarks

A hierarchal mechanism for reaction of RONS with bacterial cells in plasma activated solutions was proposed as an evaluator for cell viability. The mechanism, based on reactions for modification of cysteine in solution, was implemented in a global plasma chemistry model to describe relationships between plasma operating parameters and time to bacterial inactivation. The mechanism was normalized to be consistent with times for bacterial inactivation reported in the literature for similar operating conditions. The consequences of inlet

gas composition in a non-touching plasma source indicated that a nitrogen addition to the inlet rare gas resulting in non-negligible production of RNS that solvate into solution leads to more rapid bacterial inactivation than only an oxygen addition. Inactivation times for a touching plasma source configuration were compared to the non-touching configuration using the same gas composition, power, and distance from the target. The touching plasma was twice as efficient at bacterial inactivation as the non-touching plasma in spite of similar ROS production in the gas-phase. However, the touching plasma produced 100 times more RNS in the air gap between the outlet of the plasma source and the liquid surface than the non-touching plasma. When the length of the air gap was varied in the touching configuration to maximize RNS delivery to the surface, cell killing became less efficient, indicating that production of both ROS and RNS are important to consider when designing effective plasma systems for bacterial inactivation.

Although the model discussed in this paper makes several simplifying assumptions (such as neglecting reactions of RONS with the cell growth medium), the capability was demonstrated to reproduce trends for bacterial inactivation reported in the literature across a range of plasma operating parameters and plasma devices. The current model is limited to planktonic bacterial cells that are free to move about in the solution. The mechanism may not be valid for treatment of eukaryotic cells, which are more complex than bacterial cells. Jablonowski *et al* observed, similarly to the findings in this work, that bacterial cell inactivation was most effective when plasma-produced ROS and RNS fluxes were delivered to the surface, but that eukaryotic cells (such as mammalian cancer cells) were less affected by the plasma activated species produced by the same gas mixture [42]. Eukaryotic cells are also often plated at the bottom of a well plate or petri dish and covered by a thin layer of solution. Needed improvements to the model to address these conditions would be adding capability to have stationary cells under the liquid layer, which would enable probable mechanisms for eukaryotic cell killing to be investigated more accurately.

Data availability statement

The data that support the findings of this study are either contained within this paper or available from the corresponding author upon reasonable request.

Acknowledgments

The authors would like to acknowledge Katharina Stapelmann and María J. Herrera-Quesada for lending their expertise in the field of plasma medicine and providing data that was the initial motivation for this work. This work was supported by the U.S. National Science Foundation (PHY-2020010, CBET-2032604). This material was also based upon work supported by the U.S. Department of Energy, Office of Science, Office of Fusion Energy Sciences under Award No. DE-SC0020232.

Conflict of interest

The authors have no conflicts of interest to disclose.

ORCID iDs

Jordyn Polito https://orcid.org/0000-0003-3409-6007
Mark J Kushner https://orcid.org/0000-0001-7437-8573

References

[1] Keidar M, Shashurin A, Volotskova O, Ann Stepp M, Srinivasan P, Sandler A and Trink B 2013 *Phys. Plasma* **20** 057101
[2] Graves D B 2014 *Plasma Process. Polym.* **11** 1120
[3] Kramer A *et al* 2013 *Clin. Plasma Med.* **1** 11
[4] Bekeschus S, Schmidt A, Weltmann K D and von Woedtke T 2016 *Clin. Plasma Med.* **4** 19
[5] Kaushik N, Mitra S, Baek E J, Nguyen L N, Bhartiya P, Kim J H, Choi E H and Kaushik N K 2023 *J. Adv. Res.* **43** 59
[6] Nicol M K J *et al* 2020 *Sci. Rep.* **10** 3066
[7] Urashima K 2022 *IEEE Open J. Nanotechnol.* **3** 159
[8] Jung J-S and Kim J-G 2017 *J. Electrost.* **86** 12
[9] Sakudo A, Yagyu Y and Onodera T 2019 *Int. J. Mol. Sci.* **20** 5216
[10] Scholtz V, Pazlarova J, Souskova H, Khun J and Julak J 2015 *Biotechnol. Adv.* **33** 1108
[11] Šimončicová J, Kryštofová S, Medvecká V, Ďurišová K and Kaliňáková B 2019 *Appl. Microbiol. Biotechnol.* **103** 5117
[12] Lackmann J-W and Bandow J E 2014 *Appl. Microbiol. Biotechnol.* **98** 6205
[13] Golda J *et al* 2016 *J. Phys. D: Appl. Phys.* **49** 084003
[14] Yahaya A G, Okuyama T, Kristof J, Blajan M G and Shimizu K 2021 *Molecules* **26** 2523
[15] Van Gils C A J, Hofmann S, Boekema B K H L, Brandenburg R and Bruggeman P J 2013 *J. Phys. D: Appl. Phys.* **46** 175203
[16] Chandana L, Sangeetha C J, Shashidhar T and Subrahmanyam C 2018 *Sci. Total Environ.* **640–641** 493
[17] Deng X, Shi J and Kong M G 2006 *IEEE Trans. Plasma Sci.* **34** 1310
[18] Zhang H, Zhang C and Han Q 2023 *Appl. Microbiol. Biotechnol.* **107** 5301
[19] Wang L, Xia C, Guo Y, Yang C, Cheng C, Zhao J, Yang X and Cao Z 2020 *Future Microbiol.* **15** 115
[20] Oliver M A, Hussein L K, Molina E A, Keyloun J W, McKnight S M, Jimenez L M, Moffatt L T, Shupp J W and Carney B C 2024 *Burns* **50** 192–1212
[21] Boekema B, Stoop M, Vlig M, van Liempt J, Sobota A, Ulrich M and Middelkoop E 2021 *Appl. Microbiol. Biotechnol.* **105** 2057
[22] Ning W, Shang H, Ji Y, Li R, Zhao L, Huang X and Jia S 2023 *High Volt.* **8** 326
[23] Lietz A M and Kushner M J 2016 *J. Phys. D: Appl. Phys.* **49** 425204
[24] Bruno G, Heusler T, Lackmann J W, von Woedtke T, Weltmann K D and Wende K 2019 *Clin. Plasma Med.* **14** 100083
[25] Attri P, Han J, Choi S, Choi E H, Bogaerts A and Lee W 2018 *Sci. Rep.* **8** 10218
[26] Polito J, Herrera Quesada M J, Stapelmann K and Kushner M J 2023 *J. Appl. Phys.* **56** 395205

[27] Kruszelnicki J, Lietz A M and Kushner M J 2019 *J. Phys. D: Appl. Phys.* **52** 355207
[28] Mai-Prochnow A, Murphy B, McLean K M, Kong M G and Ostrikov K 2014 *Int. J. Antimicrob. Agents* **43** 508
[29] Lunov O, Zablotskii V, Churpita O, Jäger A, Polívka L, Syková E, Dejneka A and Kubinová Š 2016 *Biomaterials* **82** 71
[30] Zheng H, Ho P-Y, Jiang M, Tang B, Liu W, Li D, Yu X, Kleckner N E, Amir A and Liu C 2016 *Proc. Natl Acad. Sci.* **113** 15000
[31] Lunov O, Churpita O, Zablotskii V, Deyneka I G, Meshkovskii I K, Jäger A, Syková E, Kubinová Š and Dejneka A 2015 *Appl. Phys. Lett.* **106** 053703
[32] Lackmann J W *et al* 2018 *Sci. Rep.* **8** 7736
[33] Girard P-M, Arbabian A, Fleury M, Bauville G, Puech V, Dutreix M and Sousa J S 2016 *Sci. Rep.* **6** 29098
[34] Arndt S *et al* 2013 *PLoS One* **8** 11
[35] Myers B, Barnat E and Stapelmann K 2021 *J. Appl. Phys.* **54** 455202
[36] Tsuji A, Kaneko Y, Takahashi K, Ogawa M and Goto S 1982 *Microbiol. Immunol.* **26** 15–24
[37] Tuttle A R, Trahan N D and Son M S 2021 *Curr. Protoc.* **1** e20
[38] Liu D X, Bruggeman P, Iza F, Rong M Z and Kong M G 2010 *Plasma Sources Sci. Technol.* **19** 025018
[39] Du Y, Nayak G, Oinuma G, Peng Z and Bruggeman P J 2017 *J. Phys. D: Appl. Phys.* **50** 145201
[40] Reuter S, Von Woedtke T and Weltmann K D 2018 *J. Phys. D: Appl. Phys.* **51** 233001
[41] Sutter J, Brettschneider J, Mamchur S, Krebs F, Gershman S and Miller V 2023 *Plasma* **6** 577
[42] Jablonowski H, Hänsch M A C, Dünnbier M, Wende K, Hammer M U, Weltmann K-D, Reuter S and von Woedtke T 2015 *Biointerphases* **10** 029506